Optical Materials 36 (2014) 1076–1082

Contents lists available at ScienceDirect

Optical Materials

journal homepage: www.elsevier.com/locate/optmat

Broadband, mid-infrared emission from Pr^{3+} doped GeAsGaSe chalcogenide fiber, optically clad

L. Sójka [a,b], Z. Tang [a], D. Furniss [a], H. Sakr [a], A. Oladeji [a], E. Bereś-Pawlik [b], H. Dantanarayana [a], E. Faber [c], A.B. Seddon [a], T.M. Benson [a], S. Sujecki [a,*]

[a] George Green Institute for Electromagnetics Research, University of Nottingham, University Park, NG7 2RD Nottingham, UK
[b] Institute of Telecommunication, Teleinformatics & Acoustics, Wroclaw University of Technology, Wybrzeze Wyspianskiego 27, 50-370 Wroclaw, Poland
[c] Microanalysis Research Facility, Department of Archaeology, University of Nottingham, University Park, NG7 2RD Nottingham, UK

ARTICLE INFO

Article history:
Received 24 July 2013
Received in revised form 20 January 2014
Accepted 28 January 2014
Available online 28 February 2014

Keywords:
Mid-infrared fiber lasers
Chalcogenide glasses

ABSTRACT

We present a study of mid-infrared photoluminescence in the wavelength range 3.5–5.5 μm emitted from Pr^{3+}: GeAsGaSe core/GeAsGaSe cladding chalcogenide fiber. The Pr^{3+} doped fiber optic preform is fabricated using extrusion and is successfully drawn to low optical loss, step-index fiber. Broadband mid-infrared photoluminescence is observed from the fiber, both under 1.55 μm or 1.94 μm wavelength excitation. Absorption, and emission, spectra of bulk glass and fiber are presented. Luminescent lifetimes are measured for the fiber and the Judd–Ofelt parameters are calculated. The radiative transition rates calculated from Judd–Ofelt theory are compared with experimental lifetimes. The observed strong broadband emission suggests that this type of fiber is a good candidate for further development to realize both fiber lasers and amplified spontaneous emission fiber sources in the mid-infrared region.

1. Introduction

The mid-infrared (IR) covers the 3–25 μm wavelength range and bright mid-IR light sources are one of the most intensively developing subjects in photonics in present. The reason for this is that such sources have many potential applications. Two widely differing examples, both requiring a bright mid-IR source, are: (i) remote-sensing of gases such as carbon dioxide and carbon monoxide (which exhibit fundamental vibrational absorption bands in the mid-IR) for monitoring fossil-fuel combustion efficiency and (ii) opening up new laser wavelengths for medical surgery to give fresh treatment strategies (human tissue has a rich signature of mid-IR absorptions) [1–4].

Mid-IR fiber sources have the advantage of good beam quality and potential for being pulsed. Commercially available, direct emission fiber lasers, based on lanthanide ion luminescence, cover the wavelength range 400 nm–3 μm. Lanthanide ions also exhibit transitions at longer wavelengths in the mid-IR, however these mid-IR radiative transitions are quenched by the host material employed in many of the currently used fibers [5–7]. For example, the most popular host material for realization of fiber lasers is silica glass. However, the phonon energy of silica is ~1100 cm^{-1} so radiative transitions at $\geqslant$2 μm wavelength are strongly quenched in this material. In order to construct a mid-IR fiber laser, host glasses of lower phonon energy are required. One candidate is the chalcogenide glass family. Chalcogenide glasses comprise one or more of the chalcogen elements: S, Se or Te, together with other additives to give sufficient chemical and mechanical durability [8–11] providing the prospect of robust photonic devices. To date, there has been a lot of work on lanthanide ion doped *sulfide* glasses, including in a fiber format [5]; here we have deliberately selected the lower phonon energy selenide chalcogenide glasses. However, the lanthanide ion doped chalcogenide glass compositions based on selenide have a tendency to devitrify on being heated above their T_g, for instance in order to carry out processing such as fiber-drawing. Therefore, our recent effort has been in studying and minimizing the crystallization during such processing [12–15] as well as minimizing the formation of lanthanide oxide impurity in the doped chalcogenide glasses. Lanthanide ions bound in a high-phonon-energy oxide local-environment are inactive mid-IR fluorophores because they undergo preferential non-radiative decay of excited states [16].

Based on this prior work, we demonstrate here the successful fiber-drawing of a low optical loss, optically clad, lanthanide ion doped fiber. This is a crucial milestone on the way towards realization of fiber lasers in the mid-IR.

We have selected praseodymium as the active lanthanide dopant; trivalent praseodymium ions in the selenide host glass exhibit strong absorption bands at 1.55 μm and 2 μm. These bands can be

* Corresponding author.
E-mail address: slawomir.sujecki@nottingham.ac.uk (S. Sujecki).

http://dx.doi.org/10.1016/j.optmat.2014.01.038
0925-3467/

readily pumped by available semiconductor laser diodes realized in the (AlGaIn)(AsSb) materials' system, and also by solid states lasers doped with erbium (III), thulium (III) and holmium (III) [17–19].

In this paper, successful fabrication of a Pr^{3+}: doped GeAsGaSe core/GeAsGaSe cladding step-index fiber is reported. The optical properties of the fabricated Pr^{3+}-doped chalcogenide fiber and bulk glass were investigated. Thus the emission and absorption spectra were recorded. Fluorescence radiative lifetimes were measured and compared with those obtained from Judd–Ofelt theory applied to bulk glass samples. The emission spectra and fluorescence radiative lifetimes measured from the fiber samples are similar to the results obtained by others for *bulk* samples [6] of similar selenide glass composition. This is good evidence for the promising photoluminescent properties of the Pr^{3+}-doped glass not being compromised during fiber-drawing.

2. Lanthanide ion doped chalcogenide glass preparation, extrusion and fiber-drawing

The 500–1500 ppmw (parts per million by weight) Pr^{3+}-doped GeAsGaSe bulk glasses, a 500 ppmw Pr^{3+}-doped GeAsGaSe core glass and an undoped GeAsGaSe cladding glass, were all made by the melt-quenching route. The ppmw are rounded for convenience and actual values were for bulk glasses: 500 ppmw (actual = 493 ppmw), 1000 ppmw (actual = 994 ppmw) and 1500 ppmw (actual = 1476 ppmw). The rounded value for the fiber was 500 ppmw (actual = 493 ppmw). Please note two points: (1) the glasses of the 500 ppmw bulk and the 500 ppmw fiber were from the same glass melt and (2) this actual concentration is only based on the batching record. For the glasses: As (7N Furakawa Denshi; further purified by heating under vacuum), Se (5N Materion; heat treated under vacuum), Ge (5N Cerac), Ga (5N Testbourne Ltd.) and Pr foil (3 N Alfa Aesar) were batched into a purified silica-glass ampoule inside a glove-box (N_2 with <0.1 ppmw H_2O and <0.1 ppmw O_2; MBraun) and the ampoule was sealed under vacuum (10^{-3} Pa). The sealed ampoule was rocked in a resistance furnace (Instron) for 12–14 h/850 °C, quenched and chalcogenide glass annealed (Instron) close to its glass transition temperature (T_g).

After annealing, the core glass and cladding chalcogenide glass boules were polished to a 1 μm finish (of the mating surfaces), co-extruded to form a step-index perform using an in-house extruder [20,21] and then the perform was fiber-drawn on a customized Heathway fiber drawing tower, inside a class-10,000 clean room. The 500 ppmw Pr^{3+}-doped GeAsGaSe core glass/GeAsGaSe cladding glass optical fiber had OD (outside diameter) of 250 μm and was not polymer-coated. Numerical apertures (NA) of 0.05 and 0.16 were calculated for the fiber at 1.94 μm and 4.52 μm wavelength, respectively. Numerical apertures were calculated from refractive indices measured using an IR VASE mid-infrared Ellipsometer (J.A. Woollam Co., Inc.) at room temperature.

Electron microprobe analysis was performed (JEOL JXA-8200 electron microprobe) on fiber cross-sections to reveal the fiber microstructure; 20 kV accelerating voltage, 10 nA beam current and a focused beam were used. The probe was calibrated using mineral or synthetic certified standard reference materials for Ge, As, Ga and Se, and 99.9% pure Pr foil (Alfa Aesar) and a theoretical detection limit of 383 ppm was found. A similar approach to fiber fabrication was used here as in [21] and, notwithstanding that the elemental mapping failed to distinguish the core and cladding glasses (see Fig. 1), we suggest from the results here and in [21] that the cladding depth here was 10 μm ± 5 μm deep. Further information on the fabrication and properties of this fiber will form a future publication [22].

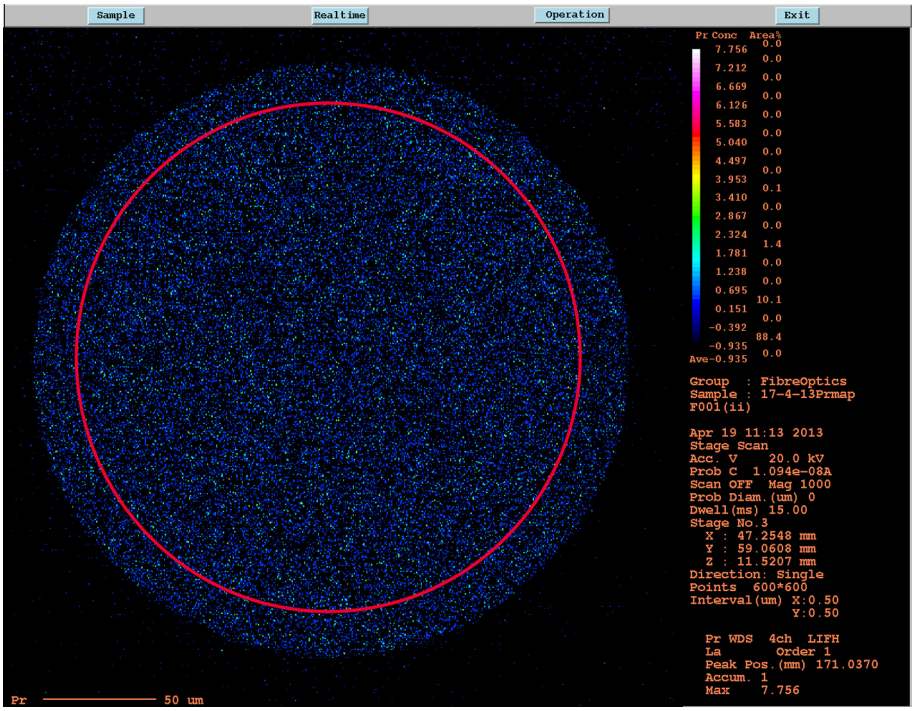

Fig. 1. Scanning electron microscopy, electron microprobe mapping analysis of a cross-section of cleaved fiber comprising Pr^{3+}: GeAsGaSe core and GeAsGaSe cladding in step-index arrangement. The figure shows elemental mapping of Pr, measured against a standard of Pr foil (99.9%, Alfa Aesar). The core and cladding were close in composition and so there was only limited evidence of the core position, shown here as a red circle. Similar results were found for the Ge, As, Ga and Se mapping. More evidence for the position drawn for the core is in [21]. (For interpretation of the references to color in this figure legend, the reader is referred to the web version of this article.)

3. Optical characterization

Absorption spectra (0.6–10 μm wavelength range) of Pr^{3+}: GeAsGaSe bulk disk samples (10 mm OD, 3 mm thick, opposite faces polished flat and parallel to a 1 μm finish) were collected using a Bruker IFS 66/S Fourier Transform Infrared Spectrometer (FTIR), which had been purged to remove both CO_2 and H_2O.

The fiber loss was measured by the cut-back method [23] using a FTIR spectrometer (IFS 66/S, Bruker). InGaAs and InSb detectors, a CaF_2 beamsplitter and tungsten source were applied for measuring the wavelength below 2.75 μm; MCT and InSb detectors, a KBr beamsplitter and globar source were engaged for measuring the wavelength range 2.75–10 μm. In this fiber loss measurement, around 2 m of fiber in total was used; there were two groups of fiber cleaves before and after the long piece cut-back (3–4 good cleaves in each group). For the calculation of the final loss spectrum (Fig. 5), the best cleave in each group was chosen by identifying the cleave which showed the highest intensity output, based on the corresponding length of fiber. All the cleaving results were checked by optical microscope during the fiber loss measurement to guarantee the measurement reliability; the error was <0.2 dB/m for the loss spectrum in Fig. 5. Please see Fig. 2 for optical photomicrographs of the two best fiber cleaves used to obtain the optical loss spectrum presented in Fig. 5. Please note that: (1) no attempt was made here to mode-strip at the launch-end of the fiber during the cut-back loss measurements, thus it is likely that there some of the light was carried in the cladding and (2) the bands at wavelengths of 1.5 μm, 1.6 μm, 2.0 μm and 4.5 μm were overloaded using the present FTIR equipment i.e. the light intensity was too low to be detected by the detector.

Room temperature fluorescence spectra were obtained in the mid-IR by pumping the step-index Pr^{3+} fiber at 1550 nm with a 100 mW fiber-coupled, single-mode laser diode (FPL 1009S Thorlabs) or at 1940 nm with a multimode laser diode with 500 mW (BA-1940-E0500-MMF200 M2K). The 1550 nm laser diode current was controlled using a LDC205C (Thorlabs) laser driver in the range of 0–500 mA while the 1940 nm laser diode was controlled using a LDC240C (Thorlabs) laser driver in the range of 0–4000 mA; the temperature of both lasers was controlled by a CAB420-15 (Thorlabs) Peltier cooler driver. A 120 mm length of Pr^{3+} doped fiber was used for the fluorescent emission measurements. Light from the laser diodes was introduced into the fiber using bulk optics. The fiber sample was mounted on a Melles Griot *xyz* translation stage to enable efficient collection of the fluorescent emission signal. The launching equipment consisted of a fiber collimator (f = 11 mm and NA = 0.25) and a microscope objective with magnification ×10 and NA = 0.2. The fluorescence was collected using a ZnSe lens and focused on the entrance slit of a monochromator. The fluorescence signal was modulated by a chopper (Scitec Instruments), since laser pump chopping gives poor lock-in due to the different lifetimes of the emission levels. The chopping frequency was in the range of 70 Hz. The emission from the chalcogenide glass fiber was passed through a motorized Spex MiniMate monochromator with diffraction-grating blazed at 6 μm (51034 JobianYvon). The detection system consisted of a lock-in amplifier (EG&G Brookdeal 9503-SC), room temperature MCT detector (Vigo System PVI-6), preamplifier for the detector (Judson PA-6) and data acquisition card (NI USB-6008 National Instruments). The monochromator and data acquisition system were controlled by means of home-written software in LabView. Emission spectra were collected over the range of wavelengths *ca.* 3–6.5 μm, at 300 K. For bulk glass measurements the sample was cut and polished to a 1 μm finish, into the form of a cuboid, with an end face 5 mm × 5 mm into which the pump laser was focused and side length 10 mm, from which the emission was collected. This allowed the laser to be focused to within 0.5 mm of the collection face and collected from within 2 mm of the launch face, so minimizing reabsorption of the emission.

Fluorescence decay was measured using the on-and-off modulation of the pump laser at 1550 nm wavelength and at 8 and10 Hz frequency. In order to try to minimize re-absorption of the emitted light, a short fiber length of ~35 mm was employed. The mid-IR lifetime decay was detected using an InSb IR detector (Judson J10D-M204B-R01M-60WL-D413/6 cooled to 77 K) in conjunction with a fast preamplifier, of response time of 100 ns, and analyzed using a digital 1 GHz oscilloscope (DPO4102B Tektronix). The decay waveforms were averaged 512×. A set of long pass filters (2 μm and 4 μm) was used to block pump power and isolate the emission. All the fluorescence decay characteristics were measured at 300 K.

4. Results

4.1. Absorption spectra

The observed room-temperature absorption spectra of the bulk glass sample series: 500 ppmw, 1000 ppmw and 1500 ppmw Pr^{3+}: GeAsGaSe in the wavelength range 1–6 μm (Fig. 3) may be

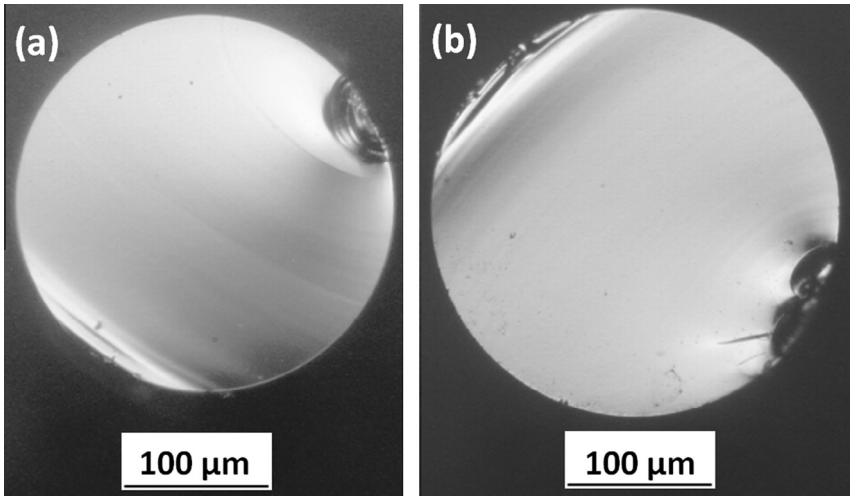

Fig. 2. Optical photomicrograph of the two best fiber cleaves used in the cut-back measurement to obtain the optical loss spectrum of the Pr^{3+}: GeAsGaSe/GeAsGaSe core/clad. Step-index fiber (Fig. 5).

interpreted using a simplified energy-level diagram of Pr^{3+} (Fig. 4, adapted from [24]). The five observed absorption bands at 1.5, 1.63, 2.04, 2.4 and 4.6 μm (Fig. 3) correspond to transitions from the ground state $^3H_4$ to the $^3F_4$, $^3F_3$, $^3F_2$, $^3H_6$, and $^3H_5$ upper levels (Fig. 4), respectively. Absorptions due to transitions from the ground state up to $^3F_4$ and $^3F_3$ strongly overlap each other, as do absorptions due to transitions from the ground state up to $^3F_2$ and $^3H_6$. However, taking into consideration the small energy difference between the levels $^3F_4$, $^3F_3$ and levels $^3F_2$, $^3H_6$, it may be assumed that both levels within each pair are in thermal equilibrium. From this assumption, the respective levels may be combined into: ($^3F_4$, $^3F_3 \rightarrow {}^3H_4$) and ($^3F_2$, $^3H_6 \rightarrow {}^3H_4$). It is important to note (Figs. 3 and 4) that Pr^{3+} ions exhibit absorption bands at 1.5 μm ($^3H_4 \rightarrow {}^3F_4$, $^3F_3$) and 2 μm ($^3H_4 \rightarrow {}^3F_2$, $^3H_6$), both of which can be efficiently pumped using commercially available laser diodes and solid state lasers.

The optical loss spectrum of the 250 μm OD, 500 ppmw Pr^{3+}: Ge–As–Ga–Se (core)/Ge–As–Ga–Se (cladding) step-index glass fiber exhibited a lowest loss of 2.8 dB/m at 6.65 μm wavelength (Fig. 5). The lowest, continuous baseline loss was ~3 dB/m over the wavelength range 6.0–7.3 μm. The absorption bands at 1.5 μm and 2 μm correspond to ground state absorption of the doped-in Pr^{3+} ions. The absorption band at 2.9 μm is assigned to O–H impurity vibrational absorption. The absorption band observed at 4.5 μm is attributed to the ground state electronic absorption band $^3H_5 \rightarrow {}^3H_4$, and also encompasses H–Se extrinsic impurity vibrational absorption.

4.2. Judd–Ofelt analysis

In order to extract the Judd–Ofelt (J–O) parameters, the absorption band spectral area for each relevant transition was calculated. The details of J–O theory and its limitations have been presented elsewhere [25–29] and are not repeated here. Five absorption bands were used here for the Judd–Ofelt computations of the Pr^{3+} parameters, at 1.5, 1.6, 2.0, 2.3 and 4.5 μm, respectively. To minimize the error, the measured FTIR absorption spectrum of each sample (500 ppmw, 1000 ppmw, 1500 ppmw Pr^{3+}: doped) was corrected by assigning three baseline functions, each represented by at least 50 selected points; the background of the spectrum was then fitted using a polynomial function. This procedure yielded nine sets of Judd–Ofelt parameters. The reduced matrix elements used in these calculations were taken from [27]. The magnetic dipole line strength was calculated from the intermediate coupled wave functions [28]. The values of the refractive

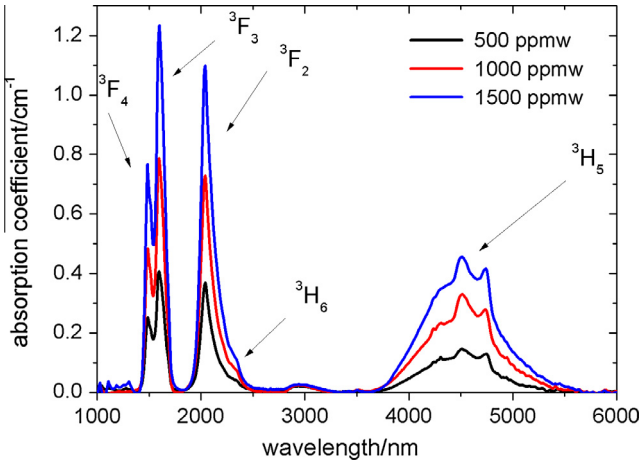

Fig. 3. Absorption spectra of 500, 1000 and 1500 ppm Pr^{3+}: GeAsGaSe bulk glasses; the upper transition state is identified in each case.

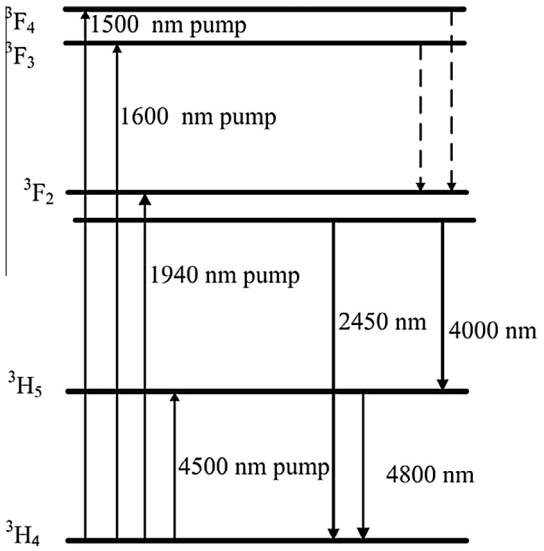

Fig. 4. Simplified, supposed energy-level diagram of Pr^{3+} in chalcogenide glass with transitions from various states identified (adapted from [24]).

index were calculated from a Sellmeier equation, where the polynomial coefficients were obtained by fitting the experimental data [30]. In order to reduce the error resulting from the baseline function extraction, an average over all nine sets of Judd–Ofelt parameters was calculated. Table 1 shows the calculated Judd–Ofelt parameters (and standard deviations) for the chalcogenide glass bulk sample Pr^{3+}: doped series. The calculated Judd–Ofelt parameters are in good agreement with literature values for Pr^{3+}: doped chalcogenide bulk glasses [6]. From the calculated Judd–Ofelt parameters, the radiative lifetimes and branching ratios were obtained. Table 2 shows the spectroscopic parameters for the relevant transitions.

4.3. Luminescence within the approximate range 3.5–5.5 μm with 1550 nm pumping

Mid-IR emission of the 500 ppm Pr^{3+} GeAsGaSe core/GeAsGaSe cladding step-index glass fiber at 3.5–5.5 μm was collected with increasing 1550 nm pump intensity (Fig. 6). A lock-in technique was employed to process the luminescence signal. A long pass filter with cut-on wavelength 2.0 μm was used in front of the exit entrance of the monochromator for measuring the mid-IR emission. The emission intensity appeared to depend linearly on the pump power intensity and there was no significant change in spectral shape with change in 1550 nm pump intensity. These findings indicate that excited state absorption and up-conversion processes may be negligible in the investigated fiber. The 3.5–5.5 μm emission band is associated with the ($^3F_2$,$^3H_6$) $\rightarrow {}^3H_5$ and $^3H_5 \rightarrow {}^3H_4$ transitions (Fig. 4). These radiative emissions overlap in energy, and are difficult to deconvolute. The dip observed in the fluorescence spectra at 4.26 μm can be attributed to ambient CO_2 absorption in the optical path. The mean emission wavelength was located at ~4.75 μm and the full-width at half maximum (FWHM) was 700 nm. This observed broad emission is desirable not only for broadband amplification but also for realization of widely tunable mid-IR lasers based on Pr^{3+}: doped GeAsGaSe fiber. Finally, we note that the mid-IR emission from the fiber was easily detected at 300 K, even with low pump power.

Fig. 7 shows the photoluminescence intensity of the 500 ppmw Pr^{3+} for both fiber and bulk samples together in order to compare their band-shapes. Note the higher noise level on the bulk sample

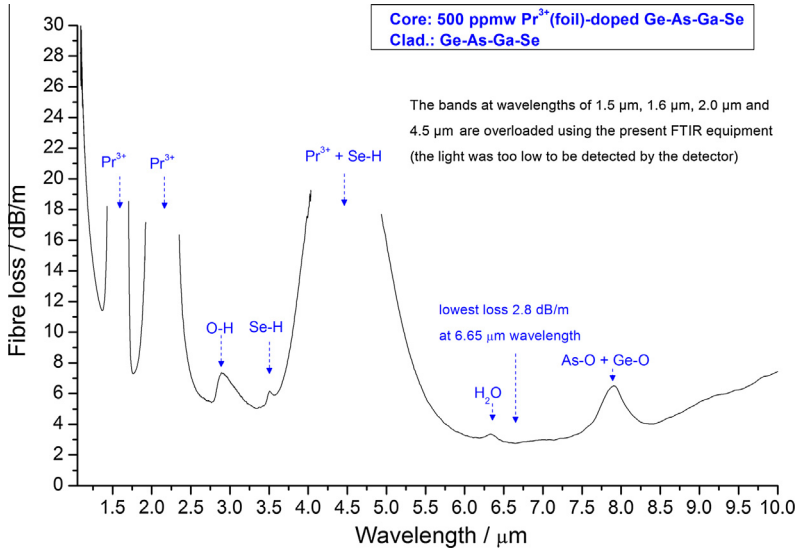

Fig. 5. Optical loss spectrum of the 500 ppm Pr^{3+}: GeAsGaSe core/GeAsGaSe clad. Step-index glass fiber drawn from the co-extruded core/clad preform.

Table 1
Calculated Judd–Ofelt parameters for bulk glass Pr^{3+} GeAsGaSe with standard deviation.

	Ω_2 (10^{-20} cm^2)	Ω_4 (10^{-20} cm^2)	Ω_6 (10^{-20} cm^2)
Pr^{3+}	9.05 ± 1.27	7.26 ± 0.92	7.28 ± 0.14

Table 2
Calculated radiative rate and branching ratio for Pr^{3+} GeAsGaSe bulk glass.

Transition	λ/(μm)	A_{ij}^{ed}/(s^{-1})	A_{ij}^{md}/(s^{-1})	τ/(ms)	β
$^3F_4 \rightarrow {}^3F_3$	22	0.11	0.008		3e−5
$^3F_4 \rightarrow {}^3F_2$	5.4	9.45			0.0026
$^3F_4 \rightarrow {}^3H_6$	3.9	378.2			0.103
$^3F_4 \rightarrow {}^3H_5$	2.1	1114.2	0.3024		0.304
$^3F_4\ {}^3H_4$	1.5	2163.9	0.8591	0.27	0.59
$^3F_3 \rightarrow {}^3F_2$	7.4	2.29	0.3		5.02e−4
$^3F_3 \rightarrow {}^3H_6$	5.1	107.4			0.0236
$^3F_3 \rightarrow {}^3H_5$	2.4	1017			0.2427
$^3F_3 \rightarrow {}^3H_4$	1.63	3343.6	2.84e−4	0.22	0.7332
$^3F_2 \rightarrow {}^3H_6$	14	1.369			6.03e−4
$^3F_2 \rightarrow {}^3H_5$	3.4	299.8			0.132
$^3F_2 \rightarrow {}^3H_4$	2.0	1969.2		0.44	0.867
$^3H_6 \rightarrow {}^3H_5$	4.7	118.6	2.14		0.44
$^3H_6 \rightarrow {}^3H_4$	2.4	152.3		3.7	0.56
$^3H_5 \rightarrow {}^3H_4$	4.9	98.5	1.85	10.0	1

response due to the much lower emission intensity of the bulk sample compared to the fiber. For convenience, the emission spectra have been normalized at 4700 nm.

It can be seen that the fiber sample exhibits a greater proportion of its observed emission intensity at wavelengths >4800 nm, compared to the bulk sample. This is to be expected due to the longer path length of the fiber sample, as follows. For emission in the fiber, the shorter wavelength emission overlaps absorption from the ground state ($^3H_5 \rightarrow {}^3H_4$). Therefore, the shorter wavelength emission is self-absorbed to be subsequently, we suggest, re-emitted at longer wavelengths.

4.4. Luminescence at 1940 nm pumping

The mid-IR emission at 3.5–5.5 μm of the 500 ppm Pr^{3+} GeAsGaSe core/GeAsGaSe cladding step-index glass fiber for increasing pump power of the 1.94 μm laser excitation is shown in Fig. 8.

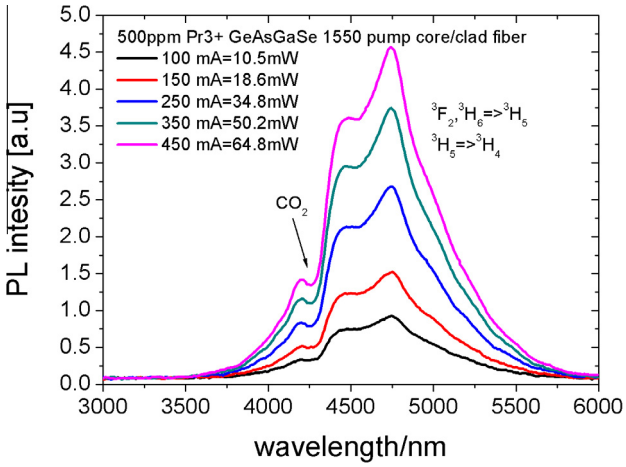

Fig. 6. Measured mid-infrared emission spectrum of the 500 ppm Pr^{3+}: GeAsGaSe core'GeAsGaSe clad. Step-index chalcogenide glass fiber using a lock-in and MCT detector (room temperature) with preamplifier and 1550 nm CW laser excitation recorded for different pump power. The emission intensities were not corrected for the system response.

Again, a lock-in technique was employed to process the luminescence signal. The emission intensity was found to depend linearly on the pump power intensity. The photoluminescence signal was strong even though the 1.94 μm wavelength is at the edge of the $^3F_2$ praseodymium (III) absorption band.

Fig. 9 compares the normalized emission spectra from ~3.5 to 5.5 μm wavelength of the 500 ppm Pr^{3+}: GeAsGaSe core/GeAsGaSe clad. chalcogenide glass fiber under 1.55 μm and 1.94 μm pumping. The spectral shape of the emission band for these two pumping wavelengths is almost identical. This result indicates that the contribution of the mid-IR infrared luminescence from the transitions ($^3F_3$, $^3F_4$) → $^3F_2$, $^3H_6$ was negligible.

4.5. Luminescence decay from ($^3F_4$, $^3F_3$)

The luminescence decay curve at 1700 nm with 1550 nm LD excitation of the 500 ppm Pr^{3+}: GeAsGaSe core/GeAsGaSe clad. chalcogenide glass fiber is shown in Fig. 10. The decay curve can be accurately fitted with a single exponential function with the

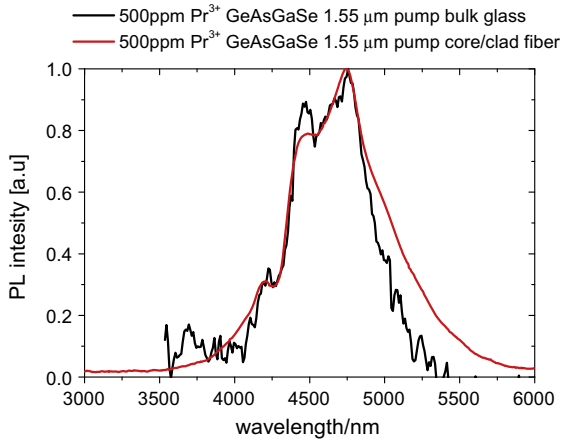

Fig. 7. Measured mid-IR emission spectrum of 500 ppm Pr^{3+}: GeAsGaSe core/GeAsGaSe clad. Step-index chalcogenide glass fiber and 500 ppm Pr^{3+} doped bulk glass GeAsGaSe sample using a lock-in and MCT detector (room temperature) with preamplifier and 1550 nm CW laser excitation. Spectra were normalized at the peak wavelength. The emission intensities were not corrected for the system response.

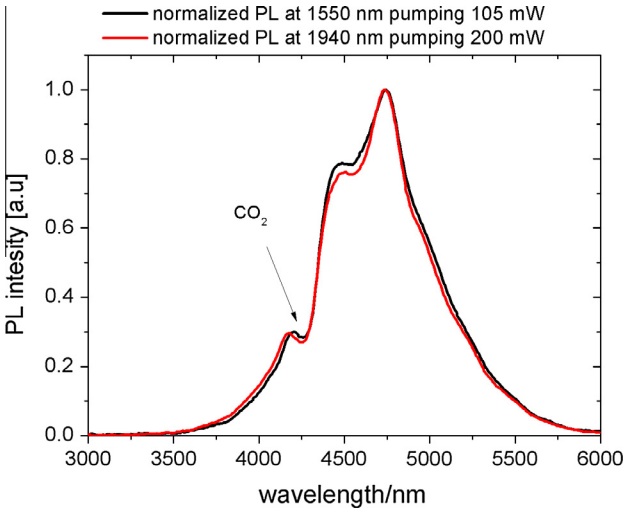

Fig. 9. Normalized emission spectra of the 500 ppm Pr^{3+}: GeAsGaSe core/GeAsGaSe clad. Step-index chalcogenide glass fiber recorded with a 1550 pump laser diode and with a 1940 nm laser diode.

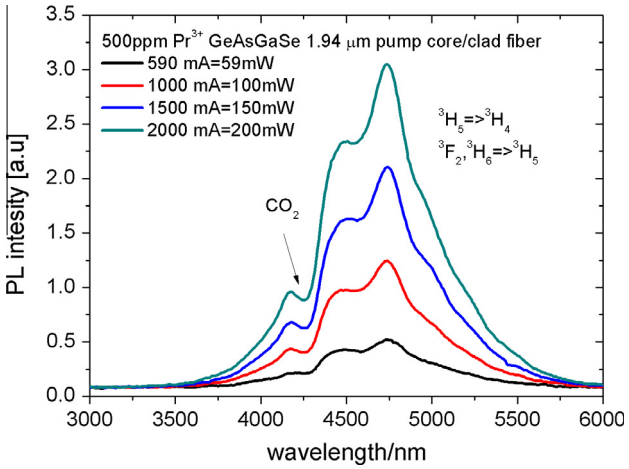

Fig. 8. Measured mid-IR emission spectrum of the 500 ppm Pr^{3+}: GeAsGaSe core/GeAsGaSe clad. Step-index chalcogenide glass fiber using a lock-in and MCT detector (room temperature) with preamplifier and 1940 nm CW laser excitation recorded for different pump power. The emission intensities were not corrected for system response.

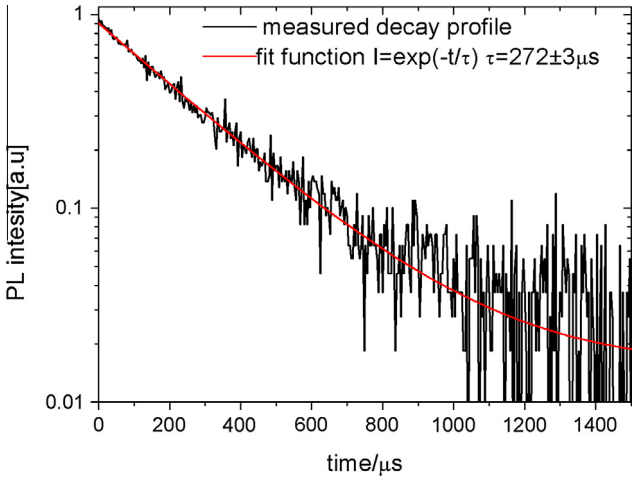

Fig. 10. Decay curve with e-folding fitting of the ($^3F_4$, $^3F_3$)–$^3H_4$ lifetime in the 500 ppm Pr^{3+}: GeAsGaSe core/GeAsGaSe clad. Step-index chalcogenide glass fiber. The red plot indicates the best fit to a single exponential. (For interpretation of the references to color in this figure legend, the reader is referred to the web version of this article.)

decay lifetime of 272 ± 3 μs. The lifetime decays were detected using a Ge detector in conjunction with a fast preamplifier and analyzed using a digital 1 GHz oscilloscope (DPO4102B Tektronix).

4.6. Luminescence decay from $^3H_5$

The fluorescence decay at 4.5–5 μm was measured by pumping a 34 mm long piece of 500 ppm Pr^{3+}: GeAsGaSe core/GeAsGaSe cladding chalcogenide glass fiber at 1550 nm with a QCW laser diode operation (Fig. 11). The fluorescence decay was recorded with low pump power intensity. Fluorescence was selected using long pass filter with a cut-on wavelength of 4 μm. This emission band can be attributed to the transitions: ($^3F_2$, $^3H_6$) → $^3H_5$ and $^3H_5$ → $^3H_4$ assuming no up-conversion to the $^1G_4$ level (low Pr^{3+} concentration). Since the ($^3F_2$, $^3H_6$) → $^3H_5$ transition decays much faster than the emission $^3H_5$ → $^3H_4$, the tail of the emission can be regarded as solely being due to the $^3H_5$ → $^3H_4$ transition [31]. The decay was fitted to a single exponential function with a lifetime of 11.52 ± 0.5 ms. The measured lifetime is in reasonable agreement with the calculated lifetime (10.0 ms) that was obtained from Judd–Ofelt theory (Table 2). Furthermore, the mid-IR measured lifetimes were found to be nearly independent of the long pass filter used. Two filters were used: one with a cut-on wavelength of 2 μm and the other with cut-on wavelength of 4 μm. Therefore, it can be concluded that the dominant contribution of the observed emission arises from the $^3H_5$ → $^3H_4$ transition. Such behavior has also been reported in the literature for Pr^{3+}:KPb_2Cl_5 and Pr^{3+}:$CsCdBr_3$ laser crystals [32,33]. Calculated and measured fluorescence spectra and lifetimes are in good agreement with the literature for Pr^{3+}-doped selenide bulk glasses [6].

Table 3 presents a comparison of the radiative lifetime obtained by Judd–Ofelt calculation (Table 2) and the measured lifetime of the ($^3F_4$, $^3F_3$ → $^3H_4$) and $^3H_5$ → $^3H_4$ transitions for the Pr^{3+}: GeAsGaSe core/GeAsGaSe cladding step-index fiber. Since the ($^3F_4$, $^3F_3$ → $^3H_4$) transitions are coupled, the radiative lifetime was calculated using a weighted contribution from each level, assuming a Boltzmann distribution. From the Boltzmann distribution, it was estimated that 90% of the excited ion population occupies the level $^3F_3$ at room temperature [6,31].

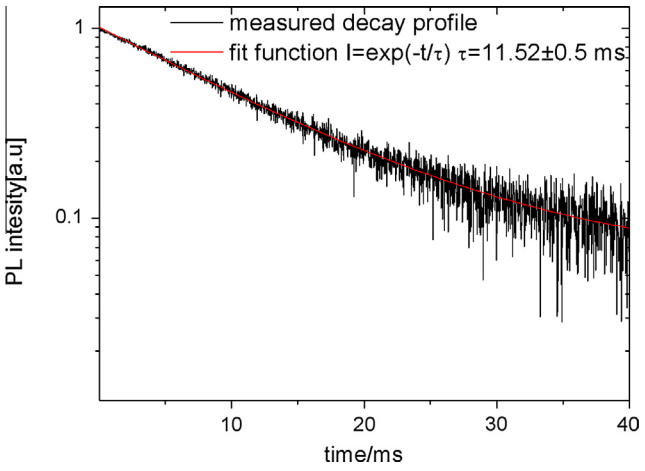

Fig. 11. Measured luminescence decay of the $^3H_5$–$^3H_4$ in 500 ppm Pr^{3+} GeAsGaSe core/GeAsGaSe cladding step-index chalcogenide glass fiber after the laser excitation at 1550 nm at 300 K. Equation the red plot indicates the best fit to a single exponential. (For interpretation of the references to color in this figure legend, the reader is referred to the web version of this article.)

Table 3
Experimental lifetime (τ_{exp}), calculated radiative lifetimes (τ_{rad}) from the J–O analysis for Pr^{3+}: GeAsGaSe core/GeAsGaSe cladding step-index chalcogenide glass fiber.

Upper state	τ_{exp} (ms)	τ_{rad} (ms)
($^3F_4$, $^3F_3$)	0.272 ± 0.003	0.23
$^3H_5$	11.5 ± 0.5	10.0

These results demonstrate that both ($^3F_4$, $^3F_3 \rightarrow {}^3H_4$) and $^3H_5 \rightarrow {}^3H_4$ transitions are radiative. The calculated quantum efficiency of these levels, defined as $\eta = \tau_{exp}/\tau_{rad}$ is close to 100%. However, there is a large error associated with the Judd–Ofelt approximation; reabsorption of the spontaneous emission in the fiber would also contribute to the error. These results support the suggestion that at least some, if not all, of the lanthanide ions have been successfully incorporated within a low phonon energy environment in the selenide glass host matrix, and were effectively isolated from impurities.

5. Conclusions

Pr^{3+} doped GeAsGaSe core/GeAsGaSe clad. step-index fiber has been successfully fabricated and its spectroscopic properties characterized. Judd–Ofelt theory has been applied using bulk doped samples for the determination of Pr^{3+} spectroscopic parameters. The radiative lifetime has been measured at 1700 nm (($^3F_4$, $^3F_3$)–$^3H_4$) and at 4.5–5 μm ($^3H_5 \rightarrow {}^3H_4$ transition dominates) compared with the theoretical lifetime calculated using Judd–Ofelt theory. Based on J–O analysis, the mid-IR emission $^3H_5 \rightarrow {}^3H_4$ efficiency was determined to be close to 100%. However, there is a large error associated with the Judd–Ofelt approximation; reabsorption of the spontaneous emission in the fiber would also contribute to the error. Broadband emission in the range of 3.5–5.5 μm from the overlapping levels ($^3F_2$, $^3H_6$) $\rightarrow {}^3H_5$ and $^3H_5 \rightarrow {}^3H_4$ was recorded for the Pr^{3+} doped GeAsGaSe core/GeAsGaSe clad. step-index glass fiber. The FWHM of the mid-IR emission was 700 nm. Measured luminescence spectra and lifetimes are in the good agreement with the results presented in the literature for Pr^{3+}-doped selenide *bulk* glasses [6]. The spectroscopic measurements show that Pr^{3+} selenide fiber is a potential candidate for the realization of broadly tunable mid-infrared fiber lasers, fiber amplifiers and ASE sources.

Acknowledgments

This research has been partly supported by the European Commission through the Framework Seven (FP7) project MINERVA (317803; www.minerva-project.eu) and partly supported by joint funding from the University of Nottingham, UK, and Wroclaw University of Technology, Poland, to support the PhD scholarship of LS.

References

[1] L. Bachmann, K. Rosa, P.A. da Ana, D.M. Zezell, A.F. Craievich, G. Kelermach, Laser Phys. Lett. 6 (2009) 159.
[2] M. Skorczakowski, J. Swiderski, P. Nyga, A. Zajac, M. Maciejewska, L. Galecki, J. Kasprzak, S. Gross, A. Heinrich, T. Bragagna, Laser Phys. Lett. 7 (2010) 498.
[3] P.A. Ann, A. Blay, W. Miyakawa, D.M. Zezell, Laser Phys. Lett. 4 (2007) 827.
[4] H. Jelinkova, O. Hohler, M. Nemec, P. Korand, J. Sulc, V. Kubecek, P. Drilik, M. Miyogi, Yi.-W. Si, Y. Matusuura, M.R. Kokto, P. Hrabal, M. Jelinek, Laser Phys. Lett. 1 (143) (2004) 143.
[5] A.B. Seddon, Z. Tang, D. Furniss, S. Sujecki, T.M. Benson, Opt. Exp. 18 (2010) 26704.
[6] L.B. Show, B. Cole, P.A. Thielen, J.S. Sanghera, I.D. Aggrawal, IEEE J. Quantum Electron 37 (2001) 1127.
[7] S. Jackson, Nat. Photonics 6 (2012) 423–431.
[8] E.M. Dianov, V.G. Plotinchenko, Y.N. Pyrkov, I.V. Smolnikov, S.A. Koleskin, G.G. Devyotykh, M.F. Churbanov, G.E. Snopatin, I.V. Skipachev, R.M. Shaposhnikov, Inorg. Mater. 39 (2003) 627.
[9] M.F. Churbanov, V.S. Shiryaev, A.I. Suchkov, A.A. Pushin, V.V. Koltasev, T.N. Pyrkov, J. Lucas, J.-L. Adam, Inorg. Mater. 43 (2007) 441.
[10] G.E. Snopatin, V.S. Shiryaev, V.G. Plotnichenka, E.M. Dianov, Inorg. Mater. 45 (2009) 1439.
[11] Z. Tang, N.C. Neate, D. Furniss, S. Sujecki, T.M. Benson, A.B. Seddon, J. Non-Cryst. Solids 357 (2453) (2011) 2453.
[12] Z. Tang, N.C. Neate, D. Furniss, S. Sujecki, T.M. Benson, A.B. Seddon, Crystallisation behaviour of Dy^{3+}-doped selenide glasses, J. Non-Cryst. Solids 357 (2011) 2453–2462.
[13] Z. Tang, D. Furniss, S. Sujecki, T.M. Benson, A.B. Seddon, The effect of the nature of the rare earth additive on chalcogenide glass stability, LASE 2011 Solid State Laser Technology, 7912:52 (Mid-IR lasers II) SPIE Photonics West, 2011.
[14] Y. Cheng, Z. Tang, N.C. Neate, D. Furniss, T.M. Benson, A.B. Seddon, The influence of dysprosium addition on the crystallization behavior of a chalcogenide selenide glass close to the fiber drawing temperature, J. Am. Ceram. Soc. 95 (12) (2012) 3834–3841.
[15] Z. Tang, D. Furniss, M. Fay, N.C. Neate, S. Sujecki, T.M. Benson, A.B. Seddon, Crystallization and optical loss studies of Dy^{3+}-doped, low ga content, selenide chalcogenide bulk glasses and optical fibers, Published Online: 21 August 2012, 2012, doi: 0.1002/9781118472590.ch23, The American Ceramic Society. Ceramic Transactions Volume 231 [Proceedings of Glass at PACRIM 9 (Cairns Australia)] Eds: A.K. Varshneya, H.A. Schaeffer, K.A. Richardson, M. Wightman, L.D. Pye.
[16] Z. Tang, D. Furniss, M. Fay, N.C. Neate, Y. Cheng, E. Barney, L. Sojka, S. Sujecki, T.M. Benson, A.B. Seddon, First identification of rare earth oxide nucleation in chalcogenide glasses and implications for fabrication of mid-infrared active fibers, J. Am. Ceram. Soc. 1–10 (2013).
[17] B.M. Walsh, Laser Phys. 20 (622) (2010) 622.
[18] S.D. Jackson, M. Pollnau, J. Li, IEEE J. Quantum Electron 47 (2011) 471.
[19] S.D. Jackson, Electron. Lett. 45 (2009) 830.
[20] K. Bhowmick, H.P. Morvan, D. Furniss, A.B. Seddon, T.M. Benson, J. Am. Ceram. Soc. 96 (2013) 118–124.
[21] S.D. Savage, C.A. Miller, D. Furniss, A.B. Seddon, J. Non-Cryst. Solids 354 (2008) 3418–3427.
[22] Z. Tang, D. Furniss, L. Sojka, S. Sujecki, T.M. Benson, E. Faber, A.B. Seddon, Fabrication and properties of praseodymium-doped chalcogenide selenide fiber, Optical Materials (Submitted for publication).
[23] K. Jinguji, M. Horiguchi, T. Manabe, Appl. Opt. 21 (4) (1982) 571.
[24] H. Dieke, H.M. Crosswhite, Appl. Opt. 2 (1963) 675.
[25] B.R. Judd, Phys. Rev. 127 (1962) 750–761.
[26] G.S. Ofelt, J. Chem. Phys. 37 (1962) 511–520.
[27] W.T. Carnall, P.R. Fields, K. Rajnak, J. Chem. Phys. 49 (1968) 4412.
[28] B.M. Walsh, J. Appl. Phys. 5 (1998) 1.
[29] Ł. Sójka, Z. Tang, H. Zhu, E. Bereś-Pawlik, D. Furniss, A.B. Seddon, T.M. Benson, S. Sujecki, Opt. Mater. Express 2 (2012) 1632–1640.
[30] H.G. Dantanarayana, A. Vukovic, P. Sewell, Z.G. Lian, D. Furniss, A.B. Seddon, E.A. Romanova, A. Konyukhov, B. Derkowska, J. Orava, T. Wagner, T.M. Benson, The optical properties of chalcogenide glasses: from measurement to electromagnetic simulation tools. in: Proceedings of the 12th International Conference on Transparent Optical Networks (ICTON 2010), June 27th – July 1st 2010, Munich, pp. 1–4.
[31] L.B. Shaw, B. Harbison, B. Cole, J. Sanghera, I. Aggarwal, Opt. Express 1 (87–96) (1997) 87–96.
[32] U. Hömmerich, E. Brown, P. Amedzake, S.B. Trivedi, J.M. Zavada, J Appl. Phys. 100 (2006) 113507.
[33] A. Ferrier, M. Velazquez, J.-L. Douoln, R. Moncorge, J. Appl. Phys. 104 (2008) 123513.